

# The nature of gravitational wave events with host environment escape velocities

GUO-PENG LI<sup>1</sup> AND XI-LONG FAN<sup>1</sup>

<sup>1</sup> *Department of Astronomy, School of Physics and Technology, Wuhan University, Wuhan 430072, China*

(Dated: February 18, 2025)

## Abstract

We propose a novel method to probe the parameters and origin channels of gravitational wave events using the escape velocities of their host environments. This method could lead to more convergent posterior distributions offering additional insights into the physical properties, formation, and evolution of the sources. It also enables testing general relativity and improves source localization, which the latter is instrumental in multi-messenger astronomy. The method provides more accurate parameter estimation for events that represent previous mergers in the hierarchical triple merger scenario and is valuable for the search for such mergers with third-generation ground-based detectors. To demonstrate this approach, we take six recently identified events in LIGO-Virgo-KAGRA data, considered as potential previous mergers in hierarchical triple mergers, as examples. The use of escape velocities results in posterior spin distributions that are concentrated near zero, aligning with the expected birth spins of first-generation black holes formed from the collapse of stars. The uncertainty in the posterior primary mass distribution is significantly reduced comparing with the LIGO-Virgo-KAGRA distributions, especially for events originating from globular clusters. We rule out the possibility that GW190512, GW170729, and GW190708 originates from globular clusters as previous mergers in the hierarchical triple merger scenario.

## 1. INTRODUCTION

The LIGO-Virgo-KAGRA (LVK) (LIGO Scientific Collaboration et al. 2015; Acernese et al. 2015; Somiya 2012; Aso et al. 2013) Collaboration has significantly advanced our understanding of the Universe, opening a new window to observe cosmic phenomena that were previously inaccessible. Accurate estimation of the parameters of gravitational wave (GW) events is crucial for several reasons. First, it allows us to determine the physical properties of the sources of these waves, such as the masses, spins, and orbital characteristics of binary systems. These parameters are key to understanding how compact objects like black holes (BHs) and neutron stars form and evolve. For instance, the mass and spin distributions of BHs provide crucial insights into their formation channels—whether these BHs result from isolated binary evolution, dynamical interactions in dense stellar environments, or hierarchical mergers (Mapelli 2021; Mandel & Farmer 2022; Gerosa & Fishbach 2021;

Arca Sedda et al. 2023). Second, accurate parameter estimation (PE) is essential for testing general relativity in the strong-field regime. This provides an opportunity to search for potential deviations from the theory, offering new insights into the limits of our current understanding of gravity. Finally, precise PE enhances our ability to localize GW sources in the sky. This is particularly important for multi-messenger astronomy, where GW detections are followed up by electromagnetic observations across the electromagnetic spectrum, spanning from radio waves to gamma rays. Identifying the host galaxies of these events provides additional context, such as the environment in which the mergers occurred, and sheds light on the role of various astrophysical processes in shaping these events. Moreover, accurate localization is vital for identifying potential counterparts, such as electromagnetic counterparts to binary BH mergers in active galactic nuclei (AGN) disks (Graham et al. 2020, 2023; Veronesi et al. 2022, 2024). In summary, accurate PE is a cornerstone of GW astronomy, enabling a deeper understanding of the Universe and driving advancements in both theoretical and observational astrophysics.

PE in GW astronomy faces several significant challenges. One primary difficulty arises from the inher-

ent noise in data collected by GW detectors (Abbott et al. 2020). These detectors are extremely sensitive, capable of measuring spacetime distortions on the order of one-thousandth the diameter of a proton. However, this sensitivity makes them highly susceptible to various noise sources, including seismic activity, thermal fluctuations, and instrumental artifacts. Distinguishing genuine GW signals from background noise requires sophisticated, computationally intensive data analysis techniques. Another major challenge is parameter degeneracy in GW signals. For example, similar waveform features can arise from different combinations of masses and spins of merging objects, complicating efforts to disentangle their individual contributions. This degeneracy often leads to large uncertainties in estimated parameters, limiting our ability to precisely characterize the sources. Additionally, the limited bandwidth of current detectors restricts the observable portion of the GW signal, further complicating the PE process.

To address these challenges, additional constraints and complementary observations are crucial. One promising approach involves incorporating information from the host environments of GW sources (Fan et al. 2014, 2017; Mo et al. 2024). For instance, the escape velocity of a host environment provides a natural constraint on the recoil (or “kick”) velocity imparted to the remnant BH due to the linear momentum carried away by GW radiation (González et al. 2007). Previous studies have made significant progress in this area by calculating the kick velocities of remnant BHs for GW events (Mahapatra et al. 2021; Varma et al. 2022). For example, GW190814 was found to have a relatively small kick velocity of  $\sim 74_{-7}^{+10}$  km s<sup>-1</sup> (Mahapatra et al. 2021), whereas GW200129 exhibited a much larger kick velocity of  $\sim 1542_{-1098}^{+747}$  km s<sup>-1</sup> (both at 90% credibility) (Varma et al. 2022). These studies have highlighted the implications of kick velocities for understanding GW events, particularly in linking remnant BH properties to their astrophysical contexts. However, most of this prior work primarily focused on quantifying kick velocities and their implications without delving deeper into the nature of GW events or systematically integrating kick constraints with other astrophysical and observational information.

In this study, we propose a novel method to constrain the parameters of GW events detected by LVK using the escape velocities of host environments. This approach not only provides a more detailed understanding of the recoil dynamics but also offers new insights into the formation channels, environments, and physical processes governing GW sources. By incorporating escape velocity as a constraint, we can more precisely

define the parameter space of GW events, significantly improving the accuracy of parameter estimation. Furthermore, we find that escape velocity serves as a constraint on the origin channels of GW events by excluding channels with distributions that deviate unreasonably from those reported by the LVK Collaboration. This methodology bridges the gap between GW observations and astrophysical theory, enabling a deeper exploration of the nature of GW events and their broader cosmological implications. Future research can build upon this framework by integrating additional astrophysical information to further enhance the accuracy and reliability of PE. This approach holds promise for unraveling the complexities of GW sources and advancing our understanding of the Universe.

## 2. HIERARCHICAL TRIPLE MERGERS

Our method is particularly well-suited for GW events that are potentially the result of previous mergers in hierarchical triple merger scenarios. The hierarchical triple merger is a specific binary BH merger scenario, proposed to occur predominantly in dynamical formation channels such as star clusters and AGN disks (Samsing & Ilan 2018, 2019). In this scenario, three BHs form a gravitationally bound three-body system, where mutual interactions facilitate the inspiral of two BHs (Campanelli et al. 2008; Lousto & Zlochower 2008). Initially, two of the BHs merge to emit a GW signal, leaving behind a remnant BH. This remnant BH subsequently forms a new binary with the third BH and merges to produce a second GW signal. Under certain orbital configurations, particularly in AGN disks due to the frequent occurrence of hierarchical mergers and the role of gas in facilitating these events, both mergers could be observed within a timescale of a few years. Recent searches (Veske et al. 2020, 2021) for hierarchical triple mergers have identified several significant merger pairs, yielding intriguing candidate families and insights into their astrophysical implications. Notably, six GW events have been identified as potential previous mergers in this scenario: GW170729, GW170818, GW170823, GW190512, GW190514, and GW190708 (Veske et al. 2021).

## 3. RETENTION VS. ESCAPE

A critical condition for hierarchical triple mergers is the retention of remnant BHs in their host environments. This requires that the kick velocities imparted to the remnants during the previous merger must be less than the escape velocities of their host environments (Mahapatra et al. 2021; Li 2022). The escape velocity is defined as the minimum speed required for an object to escape the gravitational influence of its host celestial body,

and it varies significantly across different astrophysical environments. For these six GW events, the posterior kick velocity samples from PE can be compared to the host environment’s escape velocity. Samples exceeding the escape velocity can be excluded, as this scenario necessitates that the remnant BHs remain gravitationally bound to their host environments to participate in subsequent mergers (assuming that dynamical N-body interactions do not play a dominant role in ejecting heavy remnant BHs). This reads following Bayes’ theorem:

$$p(\boldsymbol{\lambda}, V_{\text{kick}}|d) \propto \mathcal{L}(d|\boldsymbol{\lambda}, V_{\text{kick}}) \pi(\boldsymbol{\lambda}) \pi(V_{\text{kick}}|\boldsymbol{\lambda}) \quad (1)$$

where  $p(\boldsymbol{\lambda}, V_{\text{kick}}|d)$  is the posterior probability distribution of the 15-dimensional binary parameters  $\boldsymbol{\lambda}$  for quasicircular binary BHs and the remnant BH kick velocity  $V_{\text{kick}}$  given the observed data  $d$ ,  $\mathcal{L}(d|\boldsymbol{\lambda}, V_{\text{kick}})$  is the likelihood function of the data given  $\boldsymbol{\lambda}$  and  $V_{\text{kick}}$  setting to be  $\mathcal{L}(d|\boldsymbol{\lambda})$ . Note that, in the future one could assign more sophisticated models taking into account the  $V_{\text{kick}}$  in the GW data analysis processes.  $\pi(\boldsymbol{\lambda})$  is the prior adopted in current GW data analysis.  $\pi(V_{\text{kick}}|\boldsymbol{\lambda})$  is the conditional prior probability distributions for  $V_{\text{kick}}$  given by:

$$\pi(V_{\text{kick}}|\boldsymbol{\lambda}) = \begin{cases} \frac{1}{V_{\text{esc}}^{\text{max}}}, & \text{if } V_{\text{kick}}(\boldsymbol{\lambda}) < V_{\text{esc}}^{\text{max}}, \\ 0, & \text{others,} \end{cases} \quad (2)$$

where  $V_{\text{esc}}^{\text{max}}$  is the upper bound for the host environment escape velocity range, and  $V_{\text{kick}}(\boldsymbol{\lambda})$  is the kick velocity, which depends only on the intrinsic parameters  $\{m_1, m_2, \chi_1, \chi_2\}$  in  $\boldsymbol{\lambda}$ , where index 1 (2) corresponds to the primary (second) BH, with  $m_{1,2}$  the masses and  $\chi_{1,2}$  the dimensionless spins. We employ the numerical relativity fitting formulas (Campanelli et al. 2007) to infer the kick  $V_{\text{kick}}(\boldsymbol{\lambda})$ , which the  $\boldsymbol{\Lambda}$  posterior samples (we directly use the samples from Gravitational-Wave Transient Catalog 2.1 (GWTC-2.1)) yield the posterior distribution of  $V_{\text{kick}}$ .

#### 4. KICK VELOCITIES

We compute the posterior distributions of the kick velocities for the remnants of six GW events and deduce the fractions of posterior samples retained within their host environments. The retention fraction can also be interpreted as the probability that the remnant BH of a merger remains bound to its host environment. This retention probability is critical for determining whether these GW events can facilitate hierarchical mergers, as only mergers with at least one retained remnant BH are considered part of hierarchical sequences.

Table 1 summarizes the kick velocities inferred for the six GW events, which span a wide range:

**Table 1.** The kick velocities and the upper limits of retention fractions (or probabilities) for the posterior samples of the six GW events identified as previous mergers in the hierarchical triple merger scenario.

Event	$V_{\text{kick}} [\text{km s}^{-1}]$	Fraction		
		AGN disks	NSCs	GCs
GW170729	$915.38^{+1223.40}_{-693.32}$	0.5487	0.3164	0.0009
GW170818	$211.92^{+146.81}_{-130.77}$	1.0000	1.0000	0.0882
GW170823	$1029.04^{+1229.74}_{-776.23}$	0.4814	0.2274	0.0033
GW190512	$526.79^{+843.99}_{-350.18}$	0.8526	0.5771	0.0046
GW190514	$819.23^{+1115.82}_{-596.36}$	0.6290	0.3263	0.0042
GW190708	$194.23^{+179.29}_{-102.92}$	1.0000	0.9983	0.0630

**Note.** Column 1: Names of the GW events. Column 2: Median and 90% credible intervals for the kick velocities. Columns 3-5: Upper limits of the retention fractions for the posterior samples, assuming the mergers occur in AGN disks, NSCs, or GCs.

$\sim 50\text{-}2500 \text{ km s}^{-1}$ . For comparison, escape velocities in dense astrophysical environments hosting BHs range from  $\mathcal{O}(10) \text{ km s}^{-1}$  for globular clusters (GCs) (Antonini & Rasio 2016) to  $\mathcal{O}(100) \text{ km s}^{-1}$  for nuclear star clusters (NSCs) (Antonini & Rasio 2016), and up to  $\sim 1000 \text{ km s}^{-1}$  in AGN disks. Using the upper bounds of these escape velocity ranges, we calculate the upper limits for the retention fractions in AGN disks, NSCs, and GCs. For instance, in GCs, samples with kick velocities exceeding  $\sim 100 \text{ km s}^{-1}$  are excluded. We find that the retention fraction decreases as the escape velocity decreases, indicating that mergers in AGN disks require the fewest samples to be removed, while mergers in GCs require the most.

Among the six events, GW170818 and GW190708 exhibit relatively low kick velocities ( $\sim 200 \text{ km s}^{-1}$ ), making them the most suitable candidates for hierarchical triple mergers. This aligns with the findings of Veske et al. (2021), which identified the pairs GW190519-GW170818 and GW190915-GW190708 as likely hierarchical triple mergers. GW170818 and GW190708 are retained with probabilities up to  $\sim 100\%$  in AGN disks and NSCs. However, in GCs, their retention probabilities drop significantly to  $\sim 8.8\%$  and  $\sim 6.3\%$ , respectively. This suggests that GCs, due to their low escape velocities, are inefficient at producing hierarchical mergers and are unlikely sites for the observed hierarchical triple mergers.

The remaining four events have relatively high kick velocities, ranging from  $\sim 527 \text{ km s}^{-1}$  to  $\sim 1029 \text{ km s}^{-1}$ . Assuming the escape velocity of the host environment is at the upper bound for GCs, their retention probabilities are  $\lesssim 0.04\%$ . In NSCs, the retention probabilities improve to  $\leq 50\%$  (but  $\sim 57.7\%$  for GW190512 with  $V_{\text{kick}} \sim 527 \text{ km s}^{-1}$ ). In AGN disks, their retention prob-

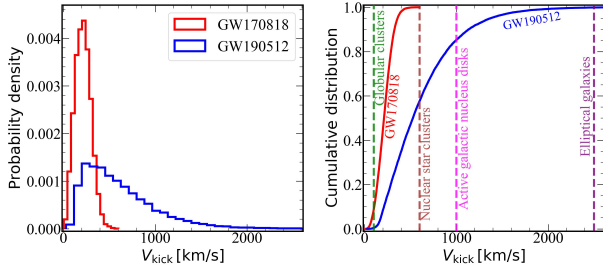


**Figure 1.** The probability distributions (left) and cumulative distributions (right) of the kick velocities for GW170818 (red) and GW190512 (blue). The vertical dotted lines represent the upper bounds of escape velocity ranges for various types of host environments, provided for comparison. The upper limit of the retention fraction (or probability) for the merger remnant is determined by the intersection of these lines with the posterior cumulative distributions.

abilities exceed  $\sim 50\%$  (but  $\sim 48.1\%$  for GW170823 with  $V_{\text{kick}} \sim 1029 \text{ km s}^{-1}$ ). These findings indicate that AGN disks, followed by NSCs, are the most promising sites for hierarchical mergers and the observation of hierarchical triple mergers, with respect with GCs.

Figure 1 illustrates the probability and cumulative distributions of kick velocities for GW170818 and GW190512, alongside fiducial escape velocities for GCs (Antonini & Rasio 2016), NSCs (Antonini & Rasio 2016), AGN disks, and giant elliptical galaxies (Merritt et al. 2004). GW170818 exhibits lower kick velocities ( $211.92^{+146.81}_{-130.77} \text{ km s}^{-1}$ , 90% credible interval), making it more likely to be retained by its host environment compared to GW190512, which has higher kick velocities ( $526.79^{+843.99}_{-350.18} \text{ km s}^{-1}$ ). Consequently, GW170818 has higher retention probabilities, reaching 100% in AGN disks and NSCs, whereas GW190512 retains probabilities of  $\sim 85.3\%$  and  $\sim 57.7\%$ , respectively, in the same environments. This suggests GW170818 is a stronger candidate for the part of hierarchical triple mergers, consistent with its significance (Veske et al. 2021).

## 5. POSTERIOR DISTRIBUTIONS

Table 2 takes GW170818 and GW190512 as examples and lists the posterior distributions ( $m_1, m_2, \chi_1, \chi_2, q, \mathcal{M}, \chi_{\text{eff}}$ , and  $\chi_p$ ), assuming these events occur within AGN disks, NSCs, or GCs. The distributions reflect the constraints imposed by the upper bounds of the escape velocity ranges of these environments (used in Table 1), illustrating the impact of host environment characteristics on the inferred parameters. We observe that as the retention fraction decreases, the distributions of the masses and spins shift toward smaller values. This trend arises because symmetric masses and lower spins result in smaller kick velocities,

which are more likely to be retained in environments with lower escape velocities.

Restricting the posterior samples based on the escape velocities of host environments leads to more convergent distributions. These constrained distributions carry additional information that aids in further determining the physical properties, formation, and evolution of the GW sources. However, as more posterior samples are excluded, the resulting distributions may deviate further from the posterior distribution obtained by the LVK Collaboration, which does not apply such priors. Significant deviations between the LVK distribution and the escape-velocity-constrained distribution can help exclude certain origin channels for GW events. To illustrate this, we analyze GW170818 and GW190512 in detail, focusing on their constrained distributions and potential origin channels.

## 6. GW170818: POSTERIOR DISTRIBUTIONS AND HOST ENVIRONMENTS

Figure 2 compares the posterior probability densities of the primary mass ( $m_1$ ) and spin magnitude ( $\chi_1$ ) for GW170818 from the GWTC-2.1 catalog (Abbott et al. 2024) and those constrained by the escape velocities of NSCs and GCs. We assume that GW170818 originates from NSCs (the upper bounds of the escape velocity ranges  $\sim 600 \text{ km s}^{-1}$ ) or GCs (that  $\sim 100 \text{ km s}^{-1}$ ). We find that if GW170818 originates from GCs,  $\sim 91\%$  of the posterior samples must be excluded due to its relatively high retention fraction in GCs. Consequently, the primary mass is better constrained from  $34.78^{+6.52}_{-4.19} M_{\odot}$  to  $33.31^{+4.14}_{-3.36} M_{\odot}$ , improving the uncertainty by  $\sim 30.1\%$  to  $\sim 22.5\%$ . The spin distribution becomes more concentrated around zero ( $\chi_1 = 0.17^{+0.35}_{-0.16}$ ), consistent with the expectation for BHs formed from stellar collapse. In contrast, the GWTC-2.1 spin distribution is nearly uniform and lacks significant information. When constrained using the upper escape velocity for NSCs, the distribution overlaps entirely with the GWTC-2.1 distribution. This is expected, as GW170818's kick velocity ( $211.92^{+146.81}_{-130.77} \text{ km s}^{-1}$ ) is well below the NSC escape velocity upper bound. These results suggest that GW170818 is likely retained in NSCs or AGN disks and may originate from such environments, while its retention in GCs is highly improbable. Meanwhile, if GW170818 originates from GCs, more convergent distributions can be obtained.

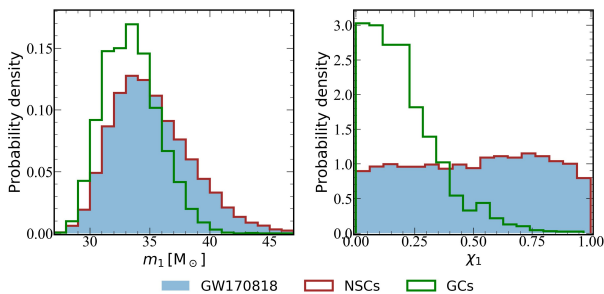
## 7. GW190512: POSTERIOR DISTRIBUTIONS AND HOST ENVIRONMENTS

Figure 3 illustrates the posterior probability densities of the primary mass and spin magnitude for GW190512.

**Table 2.** The posterior distributions of GW170818 and GW190512 for various types of host environments, including AGN disks, NSCs, and GCs.

Event	Host	$m_1 [M_\odot]$	$m_2 [M_\odot]$	$\chi_1$	$\chi_2$	$q$	$\mathcal{M} [M_\odot]$	$\chi_{\text{eff}}$	$\chi_p$
GW170818	...	$34.78^{+6.52}_{-4.19}$	$27.60^{+4.15}_{-5.10}$	$0.52^{+0.41}_{-0.47}$	$0.48^{+0.46}_{-0.42}$	$0.80^{+0.18}_{-0.24}$	$26.83^{+2.32}_{-2.00}$	$-0.06^{+0.19}_{-0.22}$	$0.56^{+0.34}_{-0.41}$
	AGN disks	$34.78^{+6.52}_{-4.19}$	$27.60^{+4.15}_{-5.10}$	$0.52^{+0.41}_{-0.47}$	$0.48^{+0.46}_{-0.42}$	$0.80^{+0.18}_{-0.24}$	$26.83^{+2.32}_{-2.00}$	$-0.06^{+0.19}_{-0.22}$	$0.56^{+0.34}_{-0.41}$
	NSCs	$34.78^{+6.52}_{-4.19}$	$27.60^{+4.15}_{-5.10}$	$0.52^{+0.41}_{-0.47}$	$0.48^{+0.46}_{-0.42}$	$0.80^{+0.18}_{-0.24}$	$26.83^{+2.32}_{-2.00}$	$-0.06^{+0.19}_{-0.22}$	$0.56^{+0.34}_{-0.41}$
	GCs	$33.31^{+4.14}_{-3.36}$	$28.59^{+3.47}_{-3.93}$	$0.17^{+0.35}_{-0.16}$	$0.24^{+0.43}_{-0.21}$	$0.87^{+0.12}_{-0.18}$	$26.72^{+2.44}_{-1.87}$	$-0.04^{+0.14}_{-0.18}$	$0.19^{+0.35}_{-0.14}$
GW190512	...	$23.15^{+5.64}_{-5.61}$	$12.53^{+3.49}_{-2.55}$	$0.20^{+0.49}_{-0.18}$	$0.40^{+0.51}_{-0.37}$	$0.54^{+0.36}_{-0.18}$	$14.56^{+1.36}_{-0.94}$	$0.02^{+0.13}_{-0.14}$	$0.26^{+0.41}_{-0.20}$
	AGN disks	$23.50^{+5.43}_{-5.66}$	$12.38^{+3.45}_{-2.47}$	$0.17^{+0.34}_{-0.15}$	$0.37^{+0.51}_{-0.33}$	$0.53^{+0.35}_{-0.17}$	$14.57^{+1.34}_{-0.95}$	$0.03^{+0.12}_{-0.13}$	$0.22^{+0.27}_{-0.17}$
	NSCs	$23.84^{+5.24}_{-5.68}$	$12.23^{+3.51}_{-2.40}$	$0.14^{+0.22}_{-0.12}$	$0.29^{+0.49}_{-0.26}$	$0.51^{+0.34}_{-0.16}$	$14.59^{+1.33}_{-0.97}$	$0.03^{+0.12}_{-0.13}$	$0.17^{+0.17}_{-0.13}$
	GCs	$18.84^{+2.52}_{-2.01}$	$15.68^{+2.26}_{-1.61}$	$0.03^{+0.10}_{-0.03}$	$0.04^{+0.08}_{-0.03}$	$0.84^{+0.13}_{-0.12}$	$15.08^{+1.09}_{-1.09}$	$-0.00^{+0.07}_{-0.05}$	$0.03^{+0.08}_{-0.02}$

**Note.** Column 1: Name of the GW events. Column 2: Host environments (AGN disks, NSCs, or GCs). Columns 3-10: Median and 90% credible intervals for the posterior distributions of  $m_1$ ,  $m_2$ ,  $\chi_1$ ,  $\chi_2$ ,  $q$ ,  $\mathcal{M}$ ,  $\chi_{\text{eff}}$ , and  $\chi_p$ . These values are obtained based on the upper limits for the retention fractions of the posterior samples retained under the assumption that the merger occurred in specific host environments. ‘...’ denotes that the posterior distributions are sourced from GWTC-2.1 (Abbott et al. 2024).



**Figure 2.** The posterior probability distributions for  $m_1$  and  $\chi_1$  of GW170818. The empty histograms represent the distributions assuming the merger takes place inside NSCs (green) or GCs (red), constrained by the upper bounds of the escape velocity ranges  $\sim 600 \text{ km s}^{-1}$  and  $\sim 100 \text{ km s}^{-1}$ , respectively. For comparison, the filled histograms (blue) illustrate the distributions from GWTC-2.1.

Assuming the event originates from AGN disks or NSCs, we observe: i) GW190512’s higher kick velocity ( $526.79^{+843.99}_{-350.18} \text{ km s}^{-1}$ ) results in retention fractions of  $\sim 85.3\%$  and  $\sim 57.7\%$  in AGN disks and NSCs, respectively. As a result, the constrained distributions are only slightly narrower than those in the GWTC-2.1 catalog; ii) The GW190512 spin distribution from GWTC-2.1 is already well-constrained and concentrated around zero, unlike GW170818. This leaves less room for further improvement through escape velocity constraints. If GW190512 originates from GCs, a noticeable deviation emerges between the primary mass distributions obtained from GWTC-2.1 and those constrained by GC escape velocities. This deviation suggests that GW190512 is unlikely to originate from GCs.

## 8. IMPLICATIONS FOR ORIGIN CHANNELS

These findings indicate that GW170818 and GW190512 likely originate from environments with

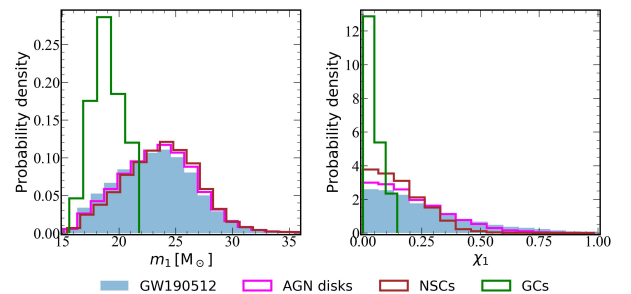


**Figure 3.** Same as Fig. 2, but for GW190512. The empty histogram (magenta) represents the posterior distribution assuming the merger takes place inside AGN disks, constrained by the upper bound of the escape velocity range. This is shown due to the higher kick velocity of GW190512,  $526.79^{+843.99}_{-350.18} \text{ km s}^{-1}$ , corresponding to the upper limit of the retention fraction in AGN disks being  $\sim 85.3\%$ .

higher escape velocities, such as NSCs or AGN disks, while GCs are less favorable. Specifically, the significant deviation in the constrained distributions of GW190512 rules out GCs as its origin channel. This conclusion further supports the use of escape velocity constraints to probe the formation and evolutionary history of GW sources, particularly in hierarchical triple merger scenarios. Conversely, once the merger comes from GCs, we can obtain its more effective posterior information.

## 9. CONCLUSIONS

In this study, we present a novel method to constrain the parameters and infer the origin channels, of GW events detected by LVK, leveraging the escape velocities of their host environments. This approach provides more accurate PE for GW events that may be the result of previous mergers in hierarchical triple merger scenarios. Additionally, it supports the search for hierarchical triple mergers using third-generation ground-based GW

detectors (Gao et al. 2024). As examples, we analyze six GW events recently identified as potential precursors in such scenarios (Veske et al. 2021).

Applying escape velocity constraints leads to more convergent posterior distributions, which carry richer information to refine our understanding of the physical properties, formation processes, and evolutionary history of the sources. This approach can also serve to test general relativity and improve source localization, which is critical for multi-messenger astronomy. Moreover, it enables the exclusion of origin channels that cause noticeable deviations between the LVK posterior distributions and those obtained under escape velocity constraints.

Our results highlight that the most credible candidates for hierarchical triple mergers tend to have lower kick velocities. In particular, by applying escape velocity constraints, the posterior spin distributions are concentrated around zero, aligning with the expected birth spin function of first-generation BHs. Among the analyzed environments, AGN disks and NSCs emerge as the most promising sites for such events (or scenarios). For GCs, we find that if GW170818 originates from GCs, the uncertainty in its posterior primary mass distribution is improved from  $\sim 30.1\%$  to  $\sim 22.5\%$ . On the other hand, GW190512 is unlikely to originate from GCs, based on the significant deviation observed in its constrained posterior distribution. The events also excluded from GC origin are GW170729 and GW190708 (see appendix B).

## 10. OUTLOOK

## APPENDIX

### A. POSTERIOR PARAMETERS

The posterior parameters in Table 2 are the primary mass  $m_1$ , the second mass  $m_2$ , the primary spin magnitude  $\chi_1$ , the second spin magnitude  $\chi_2$ , the mass ratio  $q$ , the chirp mass  $\mathcal{M}$ , the effective spin  $\chi_{\text{eff}}$ , and the effective precession parameter  $\chi_p$  of a merger. In particular,

$$q = \frac{m_2}{m_1}, \quad (\text{A1})$$

where  $m_2 \leq m_1$ ;

$$\mathcal{M} = \frac{(m_1 m_2)^{3/5}}{(m_1 + m_2)^{1/5}}; \quad (\text{A2})$$

$$\chi_{\text{eff}} = \frac{m_1 \chi_1 \cos \theta_1 + m_2 \chi_2 \cos \theta_2}{m_1 + m_2}, \quad (\text{A3})$$

where  $\theta_i$  is the misalignment angle of each BH in a merger;

$$\chi_p = \max \left[ \chi_1 \sin \theta_1, \chi_2 \sin \theta_2 \frac{q(4q+3)}{4+3q} \right]. \quad (\text{A4})$$

Previously, we highlighted the challenges of effectively inferring detailed information about the host environment solely from the distribution of binary BH merger parameters, especially when multiple formation channels are considered (Li & Fan 2024). Fortunately, this study demonstrates that the escape velocity of the host environment can be used inversely to probe the nature of GW events, offering a novel approach to address these challenges. Future work can refine this method by incorporating more precise modeling of kick velocity distributions across different environments and their influence on PE. With the deployment of third-generation GW detectors (Punturo et al. 2010a,b; Abbott et al. 2017), this approach can be extended to a broader range of events, systematically enhancing the search for hierarchical triple mergers. Furthermore, combining this method with multi-messenger astronomy—using precise source localization and joint electromagnetic observations—offers an opportunity to deepen our understanding of the formation mechanisms, environmental conditions, and cosmological implications of such events. Finally, applying this technique to special GW events, such as those with higher masses or complex spin properties, will provide new perspectives for testing general relativity and exploring the evolution of the cosmos.

### 11. ACKNOWLEDGMENTS

This work is supported by National Key R&D Program of China (2020YFC2201400), the National Natural Science Foundation of China (grant No. 11922303). **Data.** We use the samples released with GWTC-2.1 and select the datasets labeled as “cosm” and “Mixed”.

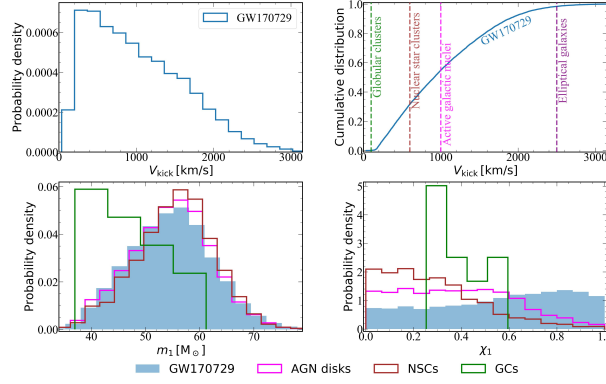


**Figure S1.** Same as Fig.1 and Fig.3, but for GW170729, showing the posterior distributions of the kick velocity (top left), primary mass (bottom left), and primary spin (bottom right), with the cumulative distribution shown in the top right. The vertical dotted lines represent the upper bounds of the escape velocity ranges for various types of host environments, provided for comparison.

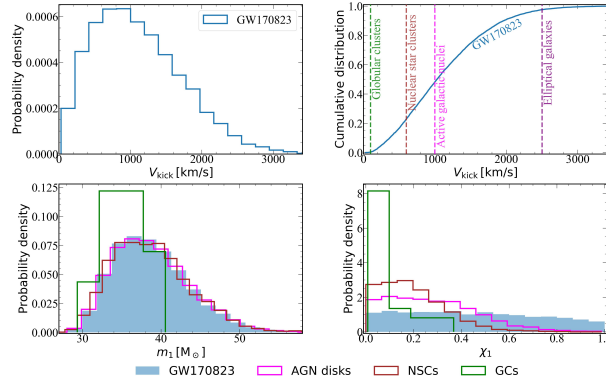


**Figure S2.** Same as Fig.S1 , but for GW170823.

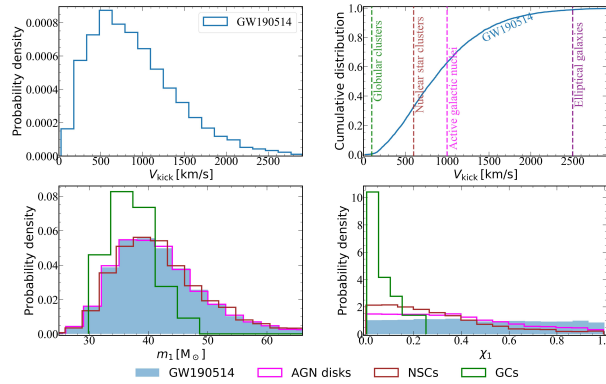


**Figure S3.** Same as Fig.S2 , but for GW190514.

## B. POSTERIOR DISTRIBUTIONS

Table S1 extends the results presented in Table 1 and Table 2 for the six GW events considered as potential previous mergers in hierarchical triple merger scenarios. The results align well with the analysis discussed in the main text.

Additionally, we provide posterior distribution plots for GW170729 (Fig. S1), GW170823 (Fig. S2), GW190514 (Fig. S3), and GW190708 (Fig. S4) that are not displayed in the main text. Notably, the data indicate that GW170729 and GW190708 are unlikely to originate from GCs in the hierarchical triple merger scenario. This conclusion is drawn

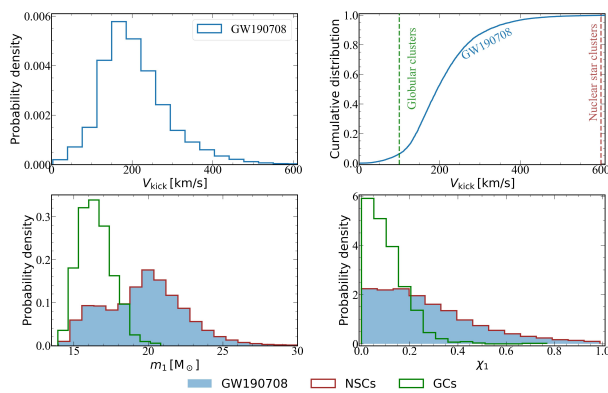


**Figure S4.** Same as Fig. S3 , but for GW190708.

from their primary mass distributions (see Figs. S1&S4), which show significant deviations from the GWTC-2.1 distributions. Such deviations suggest that the environmental constraints imposed by GCs are inconsistent with the physical characteristics of these events.



**Table S1.** Same as Table 2, but for the six GW events identified as previous mergers in the hierarchical triple merger scenario, obtained under the assumption that the merger takes place inside host environments with the various kick velocities.

Event	$V_{\text{esc}}$ [km s $^{-1}$ ]	$f_{\text{ret}}$	$m_1$ [ $M_{\odot}$ ]	$m_2$ [ $M_{\odot}$ ]	$\chi_1$	$\chi_2$	$q$	$\mathcal{M}$ [ $M_{\odot}$ ]	$\chi_{\text{eff}}$	$\chi_{\text{p}}$
	...	...	54.68 $^{+12.73}_{-12.77}$	30.20 $^{+11.95}_{-10.16}$	0.60 $^{+0.35}_{-0.53}$	0.48 $^{+0.46}_{-0.44}$	0.55 $^{+0.37}_{-0.22}$	34.55 $^{+6.97}_{-5.72}$	0.29 $^{+0.25}_{-0.33}$	0.39 $^{+0.40}_{-0.29}$
GW170729	1000	0.5487	55.04 $^{+11.59}_{-13.24}$	27.89 $^{+13.70}_{-9.12}$	0.38 $^{+0.43}_{-0.34}$	0.44 $^{+0.49}_{-0.21}$	0.51 $^{+0.41}_{-0.20}$	33.36 $^{+7.38}_{-5.31}$	0.20 $^{+0.31}_{-0.21}$	0.26 $^{+0.29}_{-0.19}$
	600	0.3164	55.84 $^{+11.00}_{-13.04}$	25.99 $^{+4.32}_{-7.98}$	0.25 $^{+0.44}_{-0.23}$	0.41 $^{+0.50}_{-0.37}$	0.47 $^{+0.42}_{-0.18}$	32.38 $^{+7.36}_{-4.81}$	0.13 $^{+0.22}_{-0.24}$	0.19 $^{+0.22}_{-0.14}$
	300	0.1035	57.10 $^{+10.86}_{-13.08}$	23.63 $^{+14.58}_{-6.59}$	0.14 $^{+0.42}_{-0.13}$	0.28 $^{+0.54}_{-0.26}$	0.42 $^{+0.43}_{-0.15}$	31.28 $^{+7.15}_{-4.35}$	0.05 $^{+0.40}_{-0.19}$	0.11 $^{+0.15}_{-0.07}$
	200	0.0334	57.07 $^{+11.53}_{-14.61}$	23.73 $^{+12.97}_{-6.94}$	0.09 $^{+0.43}_{-0.08}$	0.18 $^{+0.48}_{-0.17}$	0.42 $^{+0.42}_{-0.17}$	31.04 $^{+7.76}_{-4.10}$	0.03 $^{+0.41}_{-0.15}$	0.06 $^{+0.11}_{-0.05}$
	100	0.0009	45.89 $^{+12.03}_{-8.37}$	34.22 $^{+4.84}_{-4.20}$	0.37 $^{+0.18}_{-0.11}$	0.39 $^{+0.13}_{-0.33}$	0.75 $^{+0.16}_{-0.16}$	33.35 $^{+7.01}_{-2.89}$	0.32 $^{+0.15}_{-0.06}$	0.08 $^{+0.06}_{-0.07}$
	50	0.0001	...	...	...	...	...	...	...	...
GW170818	...	...	34.78 $^{+6.52}_{-4.19}$	27.60 $^{+4.15}_{-5.10}$	0.59 $^{+0.41}_{-0.47}$	0.48 $^{+0.46}_{-0.42}$	0.80 $^{+0.18}_{-0.24}$	26.83 $^{+2.32}_{-2.00}$	-0.06 $^{+0.19}_{-0.22}$	0.56 $^{+0.34}_{-0.41}$
	1000	1.0000	34.78 $^{+6.52}_{-4.19}$	27.60 $^{+4.15}_{-5.10}$	0.59 $^{+0.41}_{-0.47}$	0.48 $^{+0.46}_{-0.42}$	0.80 $^{+0.18}_{-0.24}$	26.83 $^{+2.32}_{-2.00}$	-0.06 $^{+0.19}_{-0.22}$	0.56 $^{+0.34}_{-0.41}$
	600	1.0000	34.78 $^{+6.52}_{-4.19}$	27.60 $^{+4.15}_{-5.10}$	0.52 $^{+0.41}_{-0.47}$	0.48 $^{+0.46}_{-0.42}$	0.80 $^{+0.18}_{-0.24}$	26.83 $^{+2.32}_{-2.00}$	-0.06 $^{+0.19}_{-0.22}$	0.56 $^{+0.34}_{-0.41}$
	300	0.8386	34.65 $^{+6.34}_{-4.12}$	27.58 $^{+4.13}_{-5.06}$	0.49 $^{+0.44}_{-0.40}$	0.44 $^{+0.49}_{-0.39}$	0.80 $^{+0.17}_{-0.24}$	26.77 $^{+2.30}_{-1.96}$	-0.06 $^{+0.18}_{-0.22}$	0.51 $^{+0.35}_{-0.38}$
	200	0.4483	34.34 $^{+6.02}_{-4.00}$	27.71 $^{+4.03}_{-4.96}$	0.30 $^{+0.42}_{-0.27}$	0.39 $^{+0.48}_{-0.35}$	0.81 $^{+0.17}_{-0.23}$	26.70 $^{+2.28}_{-1.90}$	-0.06 $^{+0.17}_{-0.21}$	0.37 $^{+0.35}_{-0.28}$
	100	0.0882	33.31 $^{+4.14}_{-3.36}$	28.59 $^{+3.47}_{-3.93}$	0.17 $^{+0.35}_{-0.16}$	0.24 $^{+0.43}_{-0.21}$	0.87 $^{+0.12}_{-0.15}$	26.72 $^{+2.44}_{-1.94}$	-0.04 $^{+0.14}_{-0.12}$	0.19 $^{+0.35}_{-0.34}$
GW170729	50	0.0108	32.01 $^{+2.33}_{-2.33}$	29.64 $^{+2.43}_{-2.43}$	0.10 $^{+0.30}_{-0.09}$	0.13 $^{+0.29}_{-0.11}$	0.94 $^{+0.05}_{-0.11}$	26.82 $^{+2.10}_{-1.65}$	-0.01 $^{+0.10}_{-0.16}$	0.11 $^{+0.26}_{-0.08}$
	...	...	38.26 $^{+9.52}_{-6.15}$	28.98 $^{+6.55}_{-7.78}$	0.44 $^{+0.48}_{-0.39}$	0.43 $^{+0.49}_{-0.39}$	0.78 $^{+0.20}_{-0.30}$	28.58 $^{+4.55}_{-3.33}$	0.05 $^{+0.21}_{-0.22}$	0.47 $^{+0.41}_{-0.35}$
	1000	0.4814	38.23 $^{+9.43}_{-6.32}$	28.55 $^{+6.72}_{-8.11}$	0.26 $^{+0.37}_{-0.23}$	0.33 $^{+0.47}_{-0.30}$	0.76 $^{+0.21}_{-0.30}$	28.24 $^{+4.64}_{-3.64}$	0.03 $^{+0.20}_{-0.22}$	0.29 $^{+0.27}_{-0.21}$
	600	0.2274	38.20 $^{+9.48}_{-6.41}$	28.51 $^{+6.35}_{-7.78}$	0.18 $^{+0.28}_{-0.12}$	0.24 $^{+0.40}_{-0.26}$	0.76 $^{+0.21}_{-0.30}$	28.20 $^{+4.51}_{-3.15}$	0.02 $^{+0.19}_{-0.12}$	0.19 $^{+0.21}_{-0.13}$
	300	0.0694	37.81 $^{+9.37}_{-6.14}$	28.58 $^{+6.12}_{-7.74}$	0.10 $^{+0.24}_{-0.09}$	0.14 $^{+0.26}_{-0.12}$	0.77 $^{+0.20}_{-0.30}$	28.10 $^{+4.23}_{-3.10}$	0.01 $^{+0.16}_{-0.16}$	0.10 $^{+0.15}_{-0.07}$
	200	0.0294	37.39 $^{+9.49}_{-5.84}$	28.99 $^{+5.62}_{-7.82}$	0.07 $^{+0.23}_{-0.06}$	0.10 $^{+0.26}_{-0.09}$	0.79 $^{+0.19}_{-0.31}$	28.14 $^{+4.05}_{-2.97}$	0.01 $^{+0.18}_{-0.12}$	0.07 $^{+0.13}_{-0.04}$
GW190512	100	0.0033	35.63 $^{+4.37}_{-5.14}$	30.61 $^{+4.10}_{-3.12}$	0.04 $^{+0.29}_{-0.03}$	0.04 $^{+0.27}_{-0.04}$	0.88 $^{+0.11}_{-0.14}$	28.59 $^{+3.29}_{-2.95}$	0.01 $^{+0.18}_{-0.10}$	0.04 $^{+0.09}_{-0.03}$
	50	0.0003	...	...	...	...	...	...	...	...
	...	...	23.15 $^{+5.64}_{-5.61}$	12.53 $^{+3.49}_{-2.55}$	0.20 $^{+0.49}_{-0.18}$	0.40 $^{+0.51}_{-0.37}$	0.54 $^{+0.36}_{-0.18}$	14.56 $^{+1.36}_{-0.94}$	0.09 $^{+0.13}_{-0.14}$	0.26 $^{+0.41}_{-0.20}$
	1000	0.8526	23.50 $^{+5.43}_{-5.66}$	12.38 $^{+3.45}_{-2.47}$	0.17 $^{+0.34}_{-0.15}$	0.37 $^{+0.51}_{-0.33}$	0.53 $^{+0.35}_{-0.17}$	14.57 $^{+1.34}_{-0.95}$	0.09 $^{+0.12}_{-0.13}$	0.22 $^{+0.27}_{-0.17}$
	600	0.5771	23.84 $^{+5.24}_{-5.68}$	12.23 $^{+3.51}_{-2.40}$	0.14 $^{+0.22}_{-0.12}$	0.29 $^{+0.49}_{-0.26}$	0.51 $^{+0.34}_{-0.18}$	14.59 $^{+1.33}_{-0.92}$	0.03 $^{+0.12}_{-0.12}$	0.17 $^{+0.17}_{-0.13}$
	300	0.2219	23.60 $^{+5.21}_{-5.67}$	12.40 $^{+3.62}_{-2.56}$	0.09 $^{+0.15}_{-0.08}$	0.16 $^{+0.35}_{-0.14}$	0.52 $^{+0.35}_{-0.17}$	14.62 $^{+1.33}_{-0.98}$	0.02 $^{+0.12}_{-0.09}$	0.09 $^{+0.11}_{-0.07}$
GW190514	200	0.0844	22.63 $^{+5.30}_{-4.90}$	12.93 $^{+3.35}_{-2.82}$	0.06 $^{+0.13}_{-0.05}$	0.09 $^{+0.23}_{-0.08}$	0.57 $^{+0.33}_{-0.19}$	14.67 $^{+1.29}_{-1.02}$	0.01 $^{+0.11}_{-0.08}$	0.05 $^{+0.08}_{-0.04}$
	100	0.0046	18.84 $^{+2.52}_{-2.01}$	15.68 $^{+2.26}_{-1.61}$	0.03 $^{+0.10}_{-0.03}$	0.04 $^{+0.08}_{-0.03}$	0.84 $^{+0.13}_{-0.12}$	15.08 $^{+1.09}_{-1.09}$	-0.00 $^{+0.07}_{-0.05}$	0.03 $^{+0.08}_{-0.02}$
	50	0.0002	...	...	...	...	...	...	...	...
	...	...	40.87 $^{+17.31}_{-9.30}$	28.35 $^{+9.96}_{-10.05}$	0.47 $^{+0.47}_{-0.42}$	0.48 $^{+0.47}_{-0.43}$	0.71 $^{+0.26}_{-0.35}$	29.14 $^{+8.08}_{-5.42}$	-0.08 $^{+0.29}_{-0.35}$	0.45 $^{+0.42}_{-0.33}$
	1000	0.6290	40.86 $^{+17.67}_{-9.43}$	27.64 $^{+9.92}_{-10.21}$	0.35 $^{+0.52}_{-0.31}$	0.40 $^{+0.51}_{-0.37}$	0.69 $^{+0.27}_{-0.36}$	28.68 $^{+7.74}_{-5.42}$	-0.10 $^{+0.27}_{-0.37}$	0.33 $^{+0.35}_{-0.24}$
	600	0.3263	40.99 $^{+19.10}_{-9.30}$	27.17 $^{+10.05}_{-10.79}$	0.24 $^{+0.53}_{-0.22}$	0.32 $^{+0.55}_{-0.29}$	0.68 $^{+0.29}_{-0.38}$	28.42 $^{+7.86}_{-5.57}$	-0.09 $^{+0.25}_{-0.39}$	0.22 $^{+0.27}_{-0.16}$
GW190708	300	0.0914	40.91 $^{+20.91}_{-9.67}$	27.27 $^{+10.36}_{-12.10}$	0.13 $^{+0.57}_{-0.12}$	0.19 $^{+0.57}_{-0.17}$	0.70 $^{+0.27}_{-0.44}$	28.40 $^{+8.01}_{-5.96}$	-0.05 $^{+0.17}_{-0.37}$	0.11 $^{+0.24}_{-0.08}$
	200	0.0355	39.77 $^{+19.90}_{-8.89}$	28.86 $^{+8.60}_{-12.32}$	0.09 $^{+0.28}_{-0.08}$	0.12 $^{+0.63}_{-0.11}$	0.75 $^{+0.22}_{-0.47}$	28.88 $^{+6.98}_{-6.00}$	-0.02 $^{+0.14}_{-0.35}$	0.08 $^{+0.16}_{-0.06}$
	100	0.0042	37.63 $^{+38.10}_{-5.74}$	31.27 $^{+9.92}_{-23.44}$	0.05 $^{+0.13}_{-0.05}$	0.08 $^{+0.68}_{-0.07}$	0.86 $^{+0.12}_{-0.76}$	30.25 $^{+6.11}_{-10.76}$	-0.02 $^{+0.11}_{-0.16}$	0.04 $^{+0.07}_{-0.03}$
	50	0.0004	...	...	...	...	...	...	...	...
	...	...	19.81 $^{+4.26}_{-4.34}$	11.61 $^{+3.08}_{-1.96}$	0.23 $^{+0.47}_{-0.20}$	0.34 $^{+0.53}_{-0.30}$	0.58 $^{+0.36}_{-0.18}$	13.05 $^{+0.86}_{-0.59}$	0.05 $^{+0.10}_{-0.10}$	0.26 $^{+0.44}_{-0.20}$
	1000	1.0000	19.81 $^{+4.26}_{-4.34}$	11.61 $^{+3.08}_{-1.96}$	0.23 $^{+0.47}_{-0.20}$	0.34 $^{+0.53}_{-0.30}$	0.58 $^{+0.36}_{-0.18}$	13.05 $^{+0.86}_{-0.59}$	0.05 $^{+0.10}_{-0.10}$	0.26 $^{+0.44}_{-0.20}$
GW190708	600	0.9983	19.81 $^{+4.26}_{-4.34}$	11.61 $^{+3.08}_{-1.96}$	0.23 $^{+0.47}_{-0.20}$	0.33 $^{+0.52}_{-0.30}$	0.58 $^{+0.36}_{-0.18}$	13.05 $^{+0.86}_{-0.59}$	0.05 $^{+0.11}_{-0.10}$	0.26 $^{+0.44}_{-0.20}$
	300	0.8709	19.91 $^{+4.29}_{-4.37}$	11.55 $^{+3.10}_{-1.94}$	0.20 $^{+0.47}_{-0.18}$	0.30 $^{+0.50}_{-0.27}$	0.58 $^{+0.36}_{-0.18}$	13.06 $^{+0.86}_{-0.60}$	0.06 $^{+0.10}_{-0.10}$	0.23 $^{+0.30}_{-0.18}$
	200	0.5285	19.56 $^{+4.36}_{-4.11}$	11.76 $^{+3.03}_{-2.06}$	0.17 $^{+0.22}_{-0.15}$	0.22 $^{+0.34}_{-0.20}$	0.60 $^{+0.35}_{-0.19}$	13.08 $^{+0.87}_{-0.62}$	0.05 $^{+0.10}_{-0.09}$	0.17 $^{+0.21}_{-0.13}$
	100	0.0630	16.37 $^{+2.09}_{-1.47}$	14.07 $^{+1.40}_{-1.56}$	0.09 $^{+0.17}_{-0.08}$	0.10 $^{+0.19}_{-0.09}$	0.86 $^{+0.12}_{-0.16}$	13.16 $^{+0.86}_{-0.67}$	0.00 $^{+0.06}_{-0.06}$	0.10 $^{+0.16}_{-0.08}$
	50	0.0125	15.70 $^{+1.46}_{-1.00}$	14.62 $^{+1.07}_{-0.86}$	0.05 $^{+0.09}_{-0.04}$	0.06 $^{+0.09}_{-0.05}$	0.94 $^{+0.06}_{-0.10}$	13.20 $^{+0.88}_{-0.66}$	-0.00 $^{+0.04}_{-0.05}$	0.06 $^{+0.07}_{-0.05}$

**Note.** Column 1: Name of the GW events. Column 2: Escape velocities of the host environments. Column 3: Retention fractions of the posterior samples that have been retained, assuming the merger takes place inside the host environment given the escape velocities. Columns 4-11: Median and 90% credible intervals for the corresponding posterior distributions of  $m_1$ ,  $m_2$ ,  $\chi_1$ ,  $\chi_2$ ,  $q$ ,  $\mathcal{M}$ ,  $\chi_{\text{eff}}$ , and  $\chi_{\text{p}}$ . ‘...’ in both  $V_{\text{kick}}$  and  $f_{\text{ret}}$  indicates that the posterior distributions are from GWTC-2.1, while other cases indicate that the number of posterior samples is too small to provide reliable median and credible intervals for the distribution.

## REFERENCES

- Abbott, B. P., Abbott, R., Abbott, T. D., et al. 2017, *Classical and Quantum Gravity*, 34, 044001, doi: [10.1088/1361-6382/aa51f4](https://doi.org/10.1088/1361-6382/aa51f4)
- . 2020, *Classical and Quantum Gravity*, 37, 055002, doi: [10.1088/1361-6382/ab685e](https://doi.org/10.1088/1361-6382/ab685e)
- Abbott, R., Abbott, T. D., Acernese, F., et al. 2024, *PhRvD*, 109, 022001, doi: [10.1103/PhysRevD.109.022001](https://doi.org/10.1103/PhysRevD.109.022001)
- Acernese, F., Agathos, M., Agatsuma, K., et al. 2015, *Classical and Quantum Gravity*, 32, 024001, doi: [10.1088/0264-9381/32/2/024001](https://doi.org/10.1088/0264-9381/32/2/024001)
- Antonini, F., & Rasio, F. A. 2016, *ApJ*, 831, 187, doi: [10.3847/0004-637X/831/2/187](https://doi.org/10.3847/0004-637X/831/2/187)
- Arca Sedda, M., Naoz, S., & Kocsis, B. 2023, *Universe*, 9, 138, doi: [10.3390/universe9030138](https://doi.org/10.3390/universe9030138)
- Aso, Y., Michimura, Y., Somiya, K., et al. 2013, *PhRvD*, 88, 043007, doi: [10.1103/PhysRevD.88.043007](https://doi.org/10.1103/PhysRevD.88.043007)
- Campanelli, M., Lousto, C., Zlochower, Y., & Merritt, D. 2007, *ApJL*, 659, L5, doi: [10.1086/516712](https://doi.org/10.1086/516712)
- Campanelli, M., Lousto, C. O., & Zlochower, Y. 2008, *Phys. Rev. D*, 77, 101501, doi: [10.1103/PhysRevD.77.101501](https://doi.org/10.1103/PhysRevD.77.101501)
- Fan, X., Messenger, C., & Heng, I. S. 2014, *ApJ*, 795, 43, doi: [10.1088/0004-637X/795/1/43](https://doi.org/10.1088/0004-637X/795/1/43)
- . 2017, *PhRvL*, 119, 181102, doi: [10.1103/PhysRevLett.119.181102](https://doi.org/10.1103/PhysRevLett.119.181102)
- Gao, B., Tang, S.-P., Yan, J., & Fan, Y.-Z. 2024, *ApJ*, 965, 80, doi: [10.3847/1538-4357/ad2e9a](https://doi.org/10.3847/1538-4357/ad2e9a)
- Gerosa, D., & Fishbach, M. 2021, *Nature Astronomy*, 5, 749, doi: [10.1038/s41550-021-01398-w](https://doi.org/10.1038/s41550-021-01398-w)
- González, J. A., Sperhake, U., Brüggmann, B., Hannam, M., & Husa, S. 2007, *PhRvL*, 98, 091101, doi: [10.1103/PhysRevLett.98.091101](https://doi.org/10.1103/PhysRevLett.98.091101)
- Graham, M. J., Ford, K. E. S., McKernan, B., et al. 2020, *PhRvL*, 124, 251102, doi: [10.1103/PhysRevLett.124.251102](https://doi.org/10.1103/PhysRevLett.124.251102)
- Graham, M. J., McKernan, B., Ford, K. E. S., et al. 2023, *ApJ*, 942, 99, doi: [10.3847/1538-4357/aca480](https://doi.org/10.3847/1538-4357/aca480)
- Li, G.-P. 2022, *A&A*, 666, A194, doi: [10.1051/0004-6361/202244257](https://doi.org/10.1051/0004-6361/202244257)
- Li, G.-P., & Fan, X.-L. 2024, arXiv e-prints, arXiv:2411.09195, doi: [10.48550/arXiv.2411.09195](https://doi.org/10.48550/arXiv.2411.09195)
- LIGO Scientific Collaboration, Aasi, J., Abbott, B. P., et al. 2015, *Classical and Quantum Gravity*, 32, 074001, doi: [10.1088/0264-9381/32/7/074001](https://doi.org/10.1088/0264-9381/32/7/074001)
- Lousto, C. O., & Zlochower, Y. 2008, *Phys. Rev. D*, 77, 024034, doi: [10.1103/PhysRevD.77.024034](https://doi.org/10.1103/PhysRevD.77.024034)
- Mahapatra, P., Gupta, A., Favata, M., Arun, K. G., & Sathyaprakash, B. S. 2021, *ApJL*, 918, L31, doi: [10.3847/2041-8213/ac20db](https://doi.org/10.3847/2041-8213/ac20db)
- Mandel, I., & Farmer, A. 2022, *PhR*, 955, 1, doi: [10.1016/j.physrep.2022.01.003](https://doi.org/10.1016/j.physrep.2022.01.003)
- Mapelli, M. 2021, in *Handbook of Gravitational Wave Astronomy*, 16, doi: [10.1007/978-981-15-4702-7\\_16-1](https://doi.org/10.1007/978-981-15-4702-7_16-1)
- Merritt, D., Milosavljević, M., Favata, M., Hughes, S. A., & Holz, D. E. 2004, *ApJL*, 607, L9, doi: [10.1086/421551](https://doi.org/10.1086/421551)
- Mo, G., Haster, C.-J., & Katsavounidis, E. 2024, arXiv e-prints, arXiv:2410.14663, doi: [10.48550/arXiv.2410.14663](https://doi.org/10.48550/arXiv.2410.14663)
- Punturo, M., Abernathy, M., Acernese, F., et al. 2010a, *Classical and Quantum Gravity*, 27, 194002, doi: [10.1088/0264-9381/27/19/194002](https://doi.org/10.1088/0264-9381/27/19/194002)
- . 2010b, *Classical and Quantum Gravity*, 27, 084007, doi: [10.1088/0264-9381/27/8/084007](https://doi.org/10.1088/0264-9381/27/8/084007)
- Samsing, J., & Ilan, T. 2018, *MNRAS*, 476, 1548, doi: [10.1093/mnras/sty197](https://doi.org/10.1093/mnras/sty197)
- . 2019, *MNRAS*, 482, 30, doi: [10.1093/mnras/sty2249](https://doi.org/10.1093/mnras/sty2249)
- Somiya, K. 2012, *Classical and Quantum Gravity*, 29, 124007, doi: [10.1088/0264-9381/29/12/124007](https://doi.org/10.1088/0264-9381/29/12/124007)
- Varma, V., Biscoveanu, S., Islam, T., et al. 2022, *PhRvL*, 128, 191102, doi: [10.1103/PhysRevLett.128.191102](https://doi.org/10.1103/PhysRevLett.128.191102)
- Veronesi, N., Rossi, E. M., van Velzen, S., & Buscicchio, R. 2022, *MNRAS*, 514, 2092, doi: [10.1093/mnras/stac1346](https://doi.org/10.1093/mnras/stac1346)
- Veronesi, N., van Velzen, S., & Rossi, E. M. 2024, arXiv e-prints, arXiv:2405.05318, doi: [10.48550/arXiv.2405.05318](https://doi.org/10.48550/arXiv.2405.05318)
- Veske, D., Márka, Z., Sullivan, A. G., et al. 2020, *MNRAS*, 498, L46, doi: [10.1093/mnras/slaa123](https://doi.org/10.1093/mnras/slaa123)
- Veske, D., Sullivan, A. G., Márka, Z., et al. 2021, *ApJL*, 907, L48, doi: [10.3847/2041-8213/abd721](https://doi.org/10.3847/2041-8213/abd721)